

SEGMENTATION AND CLASSIFICATION OF CALCIFICATION AND HEMORRHAGE IN THE BRAIN USING FUZZY C-MEAN AND ADAPTIVE NEURO- FUZZY INFERENCE SYSTEM

QAISAR JAVIAD *, MUHAMMAD ARIF**, SHAHNAWAZ TALPUR ***

*Department of Computer Science & SE, International Islamic University Islamabad, Pakistan

**Department of Computer Science, University of Gujrat, Gujrat, Pakistan

***Department of Computer Systems Engineering, Mehran University of Engineering & Technology, Jamshoro.

gaisar@iiu.edu.pk, m.arif@uog.edu.pk, shahnawaz.talpur@faculty.muuet.edu.pk,

ABSTRACT

In addition to the acquisition of excessive and false positive rates, radiotherapists tend to neglect a considerable number of deformities. The identification of features from images, along with their processing by using a pattern detection algorithm, is required in image processing. This work developed a method on the basis of the adaptive fuzzy c-mean (AFCM) method and adaptive neuro-fuzzy inference system (ANFIS). The developed method considers selective parameters, which present a major challenge in differentiating hemorrhage and calcification. ANFIS can be considered an extension of the artificial neural network family and it exhibits excellent learning skills and estimation competencies. Thus, ANFIS is a highly productive tool that can effectively manage ambiguities in any system. In medical descriptions used by radiologists, the newly recommended AFCM is desirable to offer extensive information for the early determination of a cure via surgery and radiation treatment. Desirable outcomes and useful information are most likely to be provided by fuzzy clustering segmentation methods. Irregular tissues in hemorrhage and calcification can be clearly identified with the aid of AFCM techniques. Generally, the recently recommended AFCM segmentation technique is applied to medical image segmentation. By applying this unsupervised segmentation algorithm, radiotherapists can reduce the effects of noise resulting from low-resolution sensors or/and from the movement of assemblies during data collection. The medical discipline benefits from the proposed system, especially through the identification of hemorrhage and calcification.

Keywords: Brain images, Calcification, Hemorrhage Fuzzy C-mean, Segmentation, ANFIS, Classification, Detection.

1. INTRODUCTION

The brain is a complex, delicate, and dominant part of the body that controls all bodily functions. Thus, the body is adversely affected by even the slightest brain injury. The skull protects the brain from injuries, but it prevents the brain from being directly observed for research. Hemorrhage exerts adverse impacts on the brain by altering the normal performance and structure of this organ. When abnormal cells and blood vessels in the brain are severed, brain hemorrhage normally occurs, and the functionality of the brain is affected by the presence of blood. In human beings, brain hemorrhage is the main cause of death related to solid tumor cancer [28].

The admission of calcium salts in necrotic tissue, in addition to the increase in calcified materials in local wounds, is described as a pathological calcification in the human body. Computed tomography (CT) systems generally reveal calcified wounds as high-density Hounsfield units containing phosphorus, calcium, potassium, silicon, zinc, and magnesium. Compared with routine magnetic resonance imaging (MRI), CT scanning performs better in spotting intracranial calcification as it functions on the basis of X-ray attenuation coefficients. The appearance of calcification, such as in T2-weighted (T2W) and T1-weighted (T1W) images, could not be positively defined by a common MRI sequence. The chemical process occurs at an extensive range of intensities[1, 2]. Traditional spin echo T1W and T2W images show calcification as low-intensity signals during

gradient echo acquisition; as a result, blood is displayed as a low signal and may thus cause confusion. The relatively low abundance of hydrogen protons in calcification compounds is the result of the low intensity of the calcification. A low signal is discharged by calcification, and thus, a low-intensity signal is observed in an image. An unusual hyper extreme appearance of calcification was reported by Tawil et al.[3] in a T1W image. The paramagnetic metal contents of a calcified material, which shortens the T1[3], are possibly the result of such an appearance. Calcification contents fluctuate, thus justifying the variable appearance of calcification in MRI. Given that Intra Cranial Hemorrhage (ICH) is a life-threatening condition, it must be quickly diagnosed and managed. Medical experts encounter challenges at times given that ICH is a dynamic process that exhibits several imaging attributes at the sub acute, hyper acute, and chronic stages[4]. Accurately spotting calcification and brain hemorrhage is important because an erroneous diagnosis can exert adverse impacts. Moreover, the brain is a highly complex and integrated structure, and its exploration via surgery thus holds key significance[5]. An intricate connection apparently exists among brain cells. Essentially, the inner structure of the brain is not only complex but also delicate. In addition, brain chemistry cannot be examined through general laboratory tests[6][7].

To spot hemorrhage and calcification, doctors rely on varying structural evidence, various clinical frameworks, and diverse academic approaches available in the clinical domain. Establishing rule-based systems[8] often seems a difficult task. In the medical field, brain calcification and hemorrhage can be diagnosed by using MRI or computer-based methodologies. The conglomerate algorithm fuzzy c-means (FCM) was introduced to the examination of patients and to the diagnosis and classification of abnormalities. A new algorithm, known as the alternative FCM (AFCM), was recently developed by Wu and Yang[9]. Comprehensive data can be acquired from medical images by using AFCM. The present study used AFCM segmentation techniques to distinguish hemorrhage and calcification in medical images of brains. Suitable information and desirable results are obtained through the AFCM segmentation methods.

The segmentation of medical images is a major step in clinical diagnosis. Different tissues can be clearly assessed from medical images through the successful application of clustering segmentation[10]. However, coinciding gray-scale intensities are always observed in most medical images of different tissues. Given the incomplete volume properties resulting from the low resolution of sensors and from the blur and noise during acquisition, suspicions across data obtained from MR images widely exist. Specifically, inherently vague memberships are found in boundaries, and tissues are not clearly delineated. Every point in a dataset is limited to just one cluster in traditional (hard) clustering techniques. Vague fitting labeled through a membership function (Mf) is delivered by frizzy sets. Consequently, medical images can be suitably segmented by using fuzzy clustering methods. In the present study, we focus on the use of FCM and AFCM techniques, in addition to the resolution of MRI segmentation ambiguity in ophthalmological scenarios.

2. RELATED WORK

Cocosco et al. proposed an adaptive method to segment brain MR images. A training set can be tailored using the pruning approach. The pathology of brain MRI and anatomical variability can be adjusted in this manner by using a segmentation method. Erroneously labeled samples delivered by previous tissue probability maps can be curtailed using minimum spanning tree. The k nearest neighbor(KNN) classifier[12] is used to group the tissues obtained from a brain MR image[11]. The major downside of this classifier is its inability to accurately classify tumors in the brain. El-Syed et al.[13] recommended the use of a hybrid technique to classify brain images as either normal or abnormal. This technique uses the discrete wavelet transform (DWT) method to extract the[13] features of brain MR images; these image features are subsequently condensed through principal component analysis (PCA). Finally, the features are classified as the final step. Classification basically includes two types of classifiers, namely, KNN and feed forward back propagation neural network. Zhang et al.[13] presented field models for the subdivision of brain MR images using the expectation-maximization algorithm and hidden

Markov random field[14].Subdividing a brain MR image is a completely mechanical and automated process. Threshold assessment is likely to drive this method, and this assessment is experimental in nature. Therefore, accurate results are obtained most of the time by using this method. The method proposed in[14]is costly. Saha et al.[15] proposed a fuzzy symmetry technique on the basis of the genetic clustering method for brain image segmentation. This technique uses fuzzy variable string length genetic point symmetry[15]for segmentation purposes. For membership role, a point symmetry-based distance is used instead of Euclidean distance. At this point, the basic goal is to regulate the optimum fuzzy partitioning of an MR image. Data are ideally separated by the maximum value of the FSym-index. A number of clusters can be formed, and a suitable fuzzy clustering of data can be achieved by using a genetic algorithm. In the current work, we suggest the use of fuzzy point balance-based cluster validity index to determine cluster quality. Dissimilar PD, T1, and T2 brain images have been used in certain experiments. This technique provides better output than the expectation–maximization algorithm and FCM. However, this technique does not properly segment brain images at times, and it does not consider spatial information. In addition, data sets containing similar points as a center for various clusters are not suitable for the application of this technique.

Ganesan et al.[16] proposed a fuzzy clustering method to divide brain MR images. In this method, the features of brain MR images are removed by the applying Haar wavelet transform of the images. We can obtain the approximate and detailed coefficients upon applying the Haar wavelet to a target image. In brain MR images, an imprecise coefficient is considered an attribute. Through brain segmentation, the application of these features can be observed. Experts use the clustering algorithm FCM for classification purposes. For each cluster, cluster centers are determined via FCM. The membership values for every data point in each cluster are assigned by the FCM. The cluster centers are iteratively reformed by the FCM to acquire the appropriate center within a dataset. The FCM aims to minimize objective functions. From the cluster center, the distance of any given

data point is represented by the objective function. The data membership value point likely weighs the cluster center. Within an image, different objects can be easily classified using the Mf matrix. We can also use this matrix to reconstruct images. We can apply the Sobel edge detection technique for output image edge detection. The strength of the clusters can be revealed with the silhouette method. The result of the proposed method was graphically illustrated by Ganesan et al., although they did not quantitatively prove that their results are enhanced. In addition, they did not compare their results with those of other methods to validate their findings[15].

Li et al. developed an FCM algorithm with a membership constraint by integrating spatial information for image segmentation[17]. This proposed algorithm and the traditional FCM algorithm exhibit unique features. By using this new technique, we acquire enhanced MR images and their corresponding spatial data under different noise levels; the same outcome cannot be realized with the authentic FCM algorithm. For tumor extraction, Ahmed et al.[18] proposed the use of brain MR images for segmentation by integrating the Perona–Malik anisotropic diffusion model for image enhancement and the k-means clustering algorithm for grouping tissues. Desirable results are observed in the application of this method to segmentation. FCM clustering[19]has been successfully applied in various fields, such as in geology, astronomy, target recognition, medical imaging, clustering of image segmentation, feature analysis, and classified designs. Moreover, FCM is referred to as an unsupervised system. The quantitative evaluation of the results of any clustering algorithm is known as cluster validity. Wang and Wang[20] developed a modified FCM algorithm by adjusting the membership weight age of each cluster and by integrating the spatial data for brain MR image segmentation. They applied this method to different MR images and achieved valid results from the MR images under different noise types. A semi-automatic segmentation technique was proposed by Dubey et al. [21] for brain tumor observation in MR images. Compared with that in propagation, level set evolution is likely to be used by specialists in segmentation, as reported in[21]. Fuzzy clustering has been

comprehensively applied and studied in various fields[19, 22].For instance, Zadeh[23] proposed fuzzy sets and realized the idea of integrating Mfs in more than two sets described by an Mf. FCM clustering algorithm is generally applied to studies involving fuzzy clustering. In recent years, medical images have been segmented using the FCM method. Moreover, brain MRI is mostly observed using FCM segmentation techniques [24–26]. The present work focuses on the segmentation of calcification and hemorrhage in brain images.

3. MATERIALS AND METHODS

Our method was tested in 20calcified, 20hemorrhagic, and 20 hemorrhagic and calcified cases. The sample images are shown in Fig. 1.

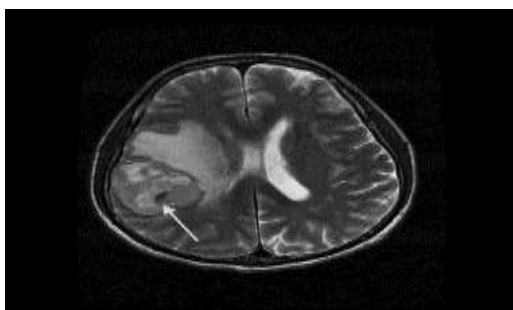


Fig. 1(a): Sample abnormal case showing hemorrhage in the MR image.



Fig. 1(b): Sample abnormal case showing calcification in the CT image

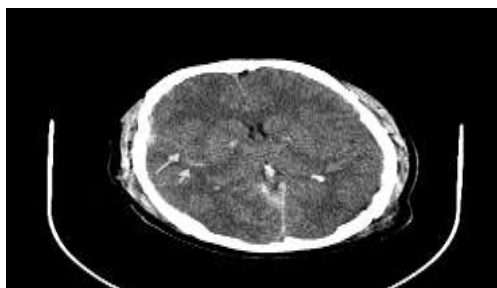


Fig. 1(c): Sample abnormal case showing hemorrhage and calcification in the CT image.

The main features of micro calcification include shape, contrast, energy, homogeneity, and correlation, which are considered in various techniques to automatically differentiate false positive and true positive measures. In addition, segmentation exerts a considerable effect on the acquisition of the abovementioned features and can ultimately assist in the classification and performance measurement. Our research work thus used segmentation to determine the precise outlines of hemorrhage and calcification and thereby maximize the information used for analysis and provide a basis for further analysis[27].

In the last few decades, the probabilistic neural network (PNN) classifier[28], artificial neural networks (ANNs)[29][30], LVQ+ANN[31],and back propagation network (BPN) classifier[32]have been widely utilized in medical image segmentation[30] and classification. In the segmentation of medical images, fuzzy clustering approaches can consider extensive mutual information related to an original image by using fuzzy membership; thus, these approaches can be used in a wide variety of applications. FCM clustering, which was established in the 1970s and later improved, assigns c membership grades and updates the membership matrix by using $c \times n$ member. Fuzzy memberships are used to update the centers that take a longer time to execute. A tight membership can be designated as pixels to update cluster centers in iterative steps and thus avoid the time and computational complexity in FCM.

- 1: For the p -dimensional input data, reorganize u_{ij} in the $d_1 \times d_2$ matrix, where d_1, d_2 are the input dimensions.
- 2: Set the new fuzzy membership functions as u_{ij}^k and the label matrix as $L = \{L^1, L^2, \dots, L^c\}$, where L^k is the label matrix of the k^{th} cluster in the present iteration.
- 3: Set all data points that are parallel to the L^k label matrix as I^k .

4: Describe $I^k = I_1^k, I_2^k, \dots, I_{nc_k}^k$ for the k^{th} cluster, where nc_k denotes the data points in the k^{th} cluster.

5: Modify the center point of the k^{th} cluster using the following equation:

$$v_k^* = \frac{\sum_{j=1}^{nc_k} I_j^k}{nc_k}$$

The fuzzy cost and membership function is calculated with the following equation.

$$u_{ij}^* = \frac{1}{\sum_{k=1}^c \left(\frac{\|x_j - v_i^*\|}{\|x_j - v_k^*\|} \right)^{2/(m-1)}}$$

$$J_m^*(U^*, V^*) = \sum_{i=1}^c \sum_{j=1}^n (u_{ij}^*)^m \|x_j - v_i^*\|^2$$

We used the fast and accurate AFCM clustering algorithm to efficiently recognize hemorrhage and calcification.

Figs. 2(a, b, and c) show the intensity graph of the sample case of hemorrhage and calcification.

Fig.2 (a): Intensity graph of hemorrhage in an MRI image.

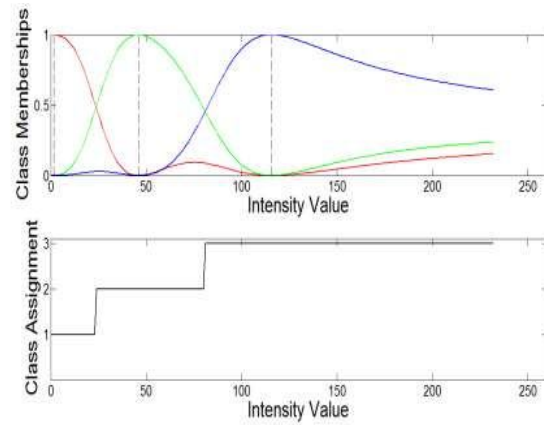


Fig.2 (b): Intensity graph of a calcification in a CT image.

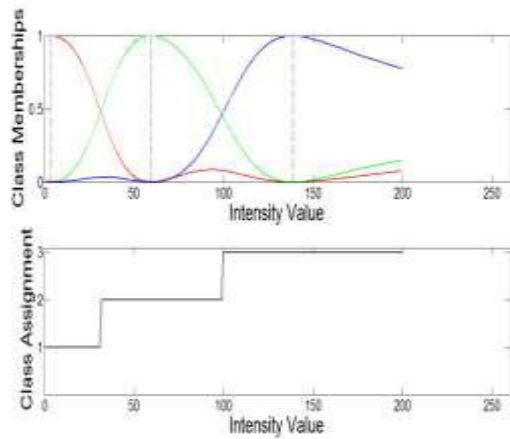


Fig.2 (c): Intensity graph of hemorrhage and calcification in a CT image.

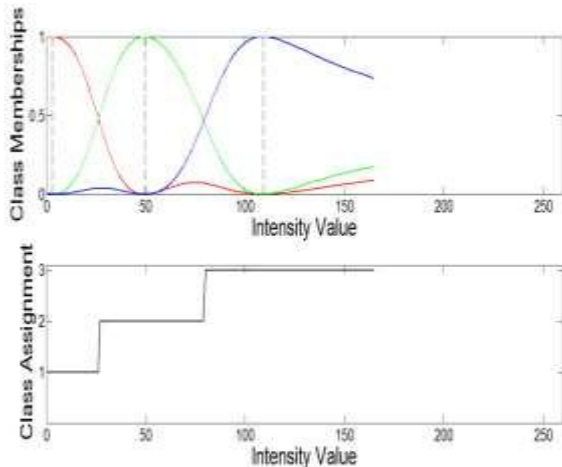


Fig.3 shows the color segmentation of calcification and hemorrhage in brain medical images.

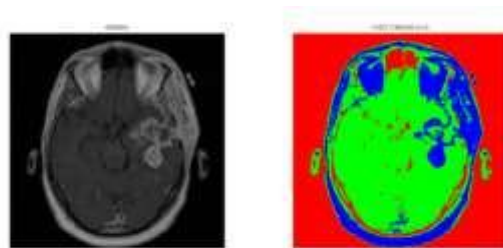


Fig. 3(a): Color clustering for hemorrhage

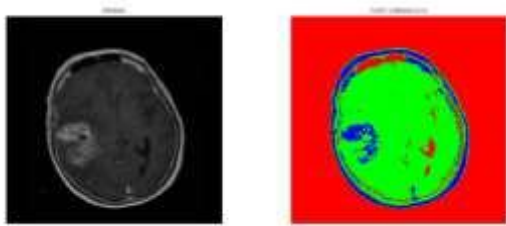


Fig. 3(b): Color clustering for hemorrhage images.

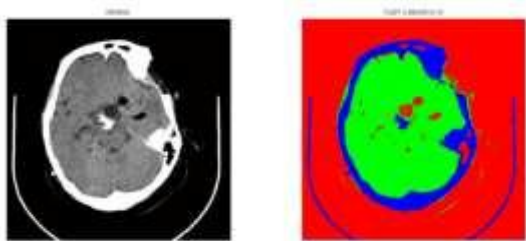


Fig. 3(b): Color clustering for calcification

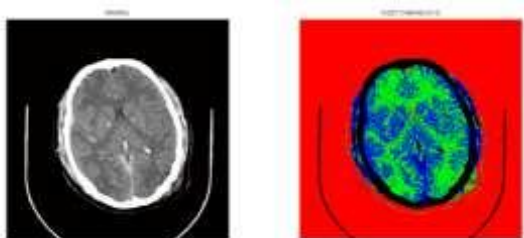


Fig. 3(d): Color clustering for calcification and hemorrhage images

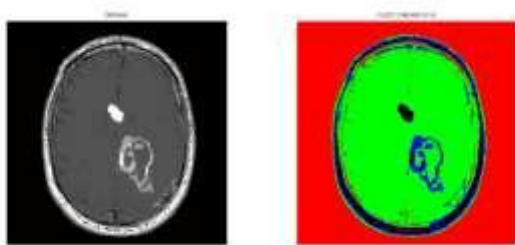


Fig. 3(e): Color clustering for calcification and hemorrhage images

We employed the AFCM on four images to show the clustering processing the calcification and hemorrhage cases.

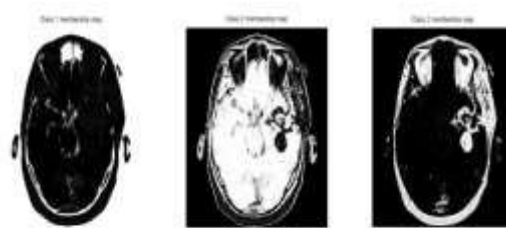


Fig. 4(a): Steps in a simple clustering of a sample hemorrhage case



Fig. 4(b): Clustering of a calcification case

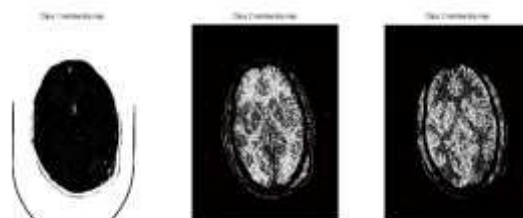


Fig. 4(c): Clustering of a calcification case

Figs. 4a–illustratethe AFCM results on the segmentation of hemorrhage and calcification cases. The succeeding step is aimed at reducing the dimensions of the AFCM results. PCA was performed to obtain the following results for dimension reduction.

GLCM was used for feature extraction after obtaining the reduction result for the AFCM dimensions. Feature extraction involves calculating the gray-level probabilities of pixels occurring in an obvious spatial association to pixels with a value j . The number of gray levels is used to determine the size of the GLCM in the whole image.

Table 1:GLCM offset values.

Offset	Angle
[0, D]	0
[-D, D]	45
[-D, 0]	90
[-D, -D]	135

We used the angles 0°, 45°, 90°, and 135° and the distances 1, 2, 3, and 4 to calculate the GLCM. The four offset values were assessed via various analyses and experiments using the stated database.

$$\sigma = \sqrt{\frac{1}{N} \sum_{i=1}^N (x_i - \mu)^2}$$

The following equation was used to calculate the standard deviation of the offset values mentioned above.

GLCM can be used to extract various statistics, which provide information on image texture. Tables 2 and 3 show the parameters used for the analysis in this part of our study. The outputs are hemorrhagic, calcified, or both hemorrhagic and calcified.

Table 2:Input and output parameters for hemorrhage and calcification segmentation

Inputs/Output	Parameter description
Input	
1	Contrast (Con)
2	Correlations (Corr)
3	Energy (Ene)
4	Homogeneity (Homo)
Output	
1	Hemorrhage
2	Calcification
3	Hemorrhagic and Calcification both

Table 3:Selected features for segmentation

Features	Description	Formulas
Contrast	The contrast feature quantifies the intensity of contrast between pixels and neighbors.	$\sum_{i,j} i - j ^2 p(i, j)$
Correlation	The correlation feature quantifies the correlation between pixels and neighbors.	$\sum_{i,j} \frac{(i - \mu_i)(j - \mu_j)p(i, j)}{\sigma_i \sigma_j}$
Energy	The energy feature quantifies the aggregation of the squared elements in GLCM.	$\sum_{i,j} p(i, j)^2$
Homogeneity	The homogeneity feature quantifies the closeness of the distributions of elements from GLCM to GLCM diagonals.	$\sum_{i,j} \frac{p(i, j)}{1 + i - j }$

Table 4 shows the evaluated features of 32 out of the 60 samples based on the selected features.

Table 4:Evaluated features of the sample images.

Input	Contrast	Correlation	Energy	Homogeneity
Image-1	10.47450426	0.556619373	0.114072025	0.187044719
Image-2	14.35417668	0.53538359	0.079166939	0.256324584
Image-3	11.12700305	0.479833457	0.11208159	0.198812244
Image-4	15.51959259	0.573584791	0.072812206	0.277135582
Image-5	11.6031588	0.565707397	0.109658119	0.207199264
Image-6	14.35412161	0.657738248	0.08843765	0.2563236

Image-7	13.37060501	0.660255513	0.102561135	0.238760804
Image-8	16.61253301	0.662841117	0.091158044	0.296652375
Image-9	12.93332844	0.647763718	0.101263616	0.230952294
Image-10	12.05911044	0.609394199	0.105968196	0.215341258
Image-11	9.32702551	0.564331884	0.11102797	0.166554027
Image-12	15.55630639	0.691493022	0.076347718	0.277791185
Image-13	14.35412161	0.671588661	0.090570847	0.2563236
Image-14	13.06093697	0.578486249	0.09795843	0.233231017
Image-15	8.927316171	0.449348687	0.109421862	0.15941636
Image-16	9.309806886	0.562464162	0.111650992	0.166246552
Image-17	7.960978409	0.43377205	0.105457546	0.142160329
Image-18	9.399166574	0.312201706	0.080297561	0.16784226
Image-19	15.28312301	0.688478787	0.081678311	0.272912911
Image-20	12.02222359	0.348558029	0.062117685	0.214682564
Image-21	8.763493303	0.436032965	0.111925123	0.156490952
Image-22	10.91152073	0.602611667	0.108936846	0.194848584
Image-23	10.1096182	0.313918928	0.075992211	0.180528896
Image-24	8.090069656	0.42263678	0.103549524	0.144348949
Image-25	10.52589251	0.527306407	0.11284473	0.188078126
Image-26	9.818632794	0.599843744	0.109656226	0.175332728
Image-27	12.5509036	0.646216833	0.10654619	0.224123279
Image-28	11.94982341	0.637584851	0.109515058	0.213389704
Image-29	14.02629571	0.66826515	0.095433116	0.250469566
Image-30	8.671252863	0.510581744	0.107901696	0.154843801
Image-31	9.7997867	0.485865631	0.110720101	0.174996191
Image-32	13.20666155	0.389669146	0.049584292	0.235833242

3.1. ADAPTIVE NEURO FUZZY INFERENCE SYSTEM (ANFIS)

Tissue segmentations classified into appropriate categories on the basis of ANFIS, which enhances the flexibility in training and is easily adaptable to the problem of emotion classification. ANFIS is an inference-based fuzzy system of neural networks that can be used to classify multi-class, nonlinear problems. In our methodology, we classified hemorrhage and calcification on the basis of the selected features with three hidden layers by using ANFIS. These layers contained 13, 9, and 5 neurons. Given the nature of neural networks, a standard method has not yet been developed to define the numbers of hidden layers and neurons. Therefore, the most effective architecture is usually

selected. The input layer contains 25 sensory neurons to match the length of the information vectors, whereas the output layer contains three neurons for classification according to seven different classes. The combination of the output neurons generates a three-digit binary sequence, and each sequence mapped to a class. The ANFIS network is trained using back propagation, which is a supervised learning technique that systematically updates the synaptic weights of multi-layer ANFIS networks. ANFIS combines all information on inputs and outputs and modifies all the information with the aid of the back propagation algorithm (Fig. 5). The ANFIS determines the target maximum velocity of the expression on the basis of the input and output training datasets. The FIS is trained and evaluated using a fuzzy logic toolbox in MATLAB.

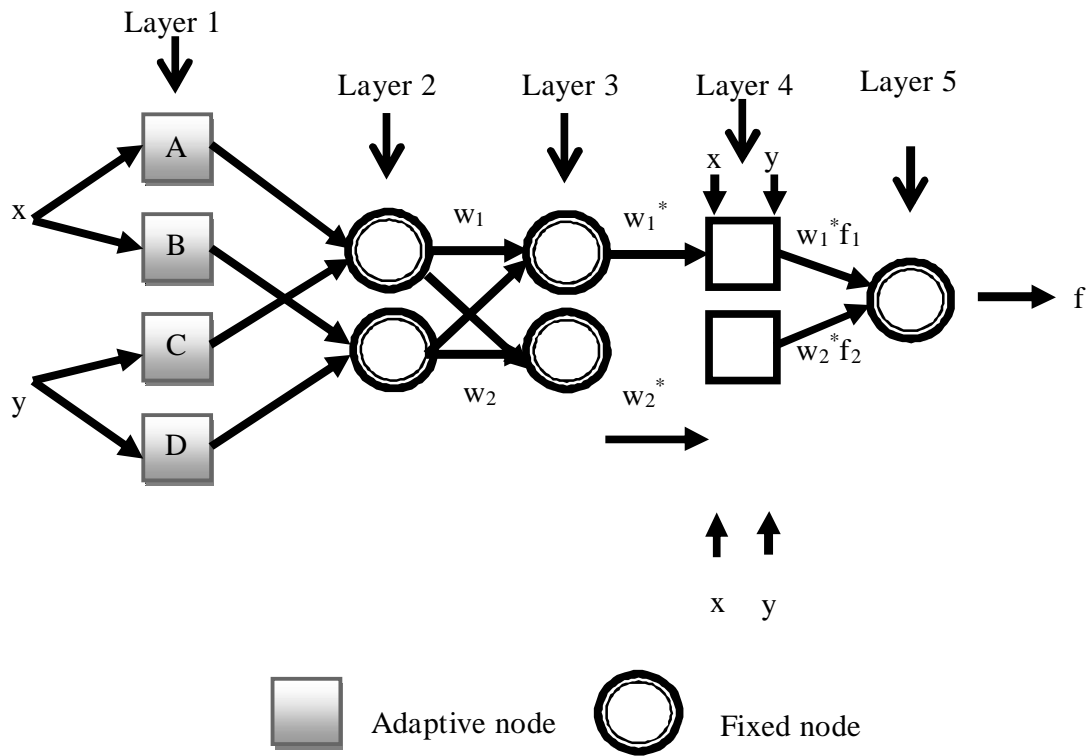


Fig. 5: ANFIS structure with two inputs, one output, and two rules

In our work, we used the first-order Sugeno model with two information inputs and the Sugeno and Takagi fuzzy rule:

$$\text{if } x \text{ is } A, \text{ then } f_1 = p_1x + t$$

The main layer in the ANFIS network comprises the Mfs and passes all information to the succeeding layer. The information is convincing textural information on hemorrhage and calcification. In this layer, every neuron is standardized with a neuron capacity.

$$O = \mu(x, y, z)$$

Where $\mu(x, y, z)_i$ denote the Mfs.

In our work, the bell-shaped Mfs with the least and greatest equivalence of 0 and 1, respectively, were selected.

$$f(x; a, b, c) = \frac{1}{1 + \left(\frac{x-c}{a}\right)^{2b}}$$

The bell-shaped function depends on parameters a, b, and c. The b parameter is characteristically positive.

In ANFIS, the second layer verifies the weights of each Mf. It recognizes the information values from the first layer, sets the Mfs, and checks the fuzzy variable information. Every neuron in the second layer duplicates the approach, is non-adjustable, and sends an item to the succeeding layer, as presented in the following equation.

$$w_i = \mu(x)_i * \mu(x)_{i+1}$$

Every neuron outputs or indicates the firing strength or weight.

The third layer in the inference system is the rule layer. The nodes map the pre-situation fuzzy rules to calculate the activation levels of each rule and to determine whether the number of layers is equal to the number of fuzzy rules. In this layer, three nodes compute the normalized weights.

The third layer in ANFIS is non-versatile, and every neuron calculates the value of the principal finishing quality to complete the principal

terminating quality, as presented in the following equation:

$$w_i^* = \frac{w_i}{w_1 + w_2}$$

$$i = 1, 2.$$

The output of the third layer is called the normalized weight or normalized terminating strength.

The fourth layer is called the de-fuzzification layer, which produces the output recovered from the third layer, known as the rule layer. Every neuron in this layer is known as a versatile neuron with a neuron capacity.

$$O_i^4 = w_i^* x f = w_i^* (p_i x + q_i y + r_i)$$

Where the parameters $\{p_i, q_i, r\}$ located in the fourth layer denote the resulting constraints.

The fifth layer is known as the yield layer, which aggregates all the input summation from the fourth layer and alters the fuzzy grouping outputs into a binary. The single neuron in the fifth layer is not versatile, and it combines all information from the fourth layer and produces results.

$$O_i^5 = \sum_i w_i^* x f = \frac{\sum_i w_i f}{\sum_i w_i}$$

ANFIS is a hybrid algorithm that is used to differentiate the parameters in a given architecture. The algorithm and its variables are run until the final parameter is identified. This process continues up to the fourth layer.

4. RESULTS

The proposed technique was developed using the MATLAB software on a Core i7 with 2.6 GHz processor. Our experiments focused on brain MRI and CT images. Our data base included tumors, hemorrhage, calcification, and edemas of different locations, orientations, sizes, shapes, and types; border-enhancing tumors; and completely enhanced and non-enhanced tumors. The edema classification step presents the images as input to

the segmentation phase. The segmentation phase of the proposed system precisely extracts the tumor region from these malignant brain images to a certain extent. Figs. 3 and 4 show the results of the segmentation phase. The effectiveness or correctness of the classifiers for every texture analysis was analyzed on the basis of the error rate. This error rate was depicted by the terms *true/false positive* and *true/false negative*.

TP (True Positive): The test result is positive for existent clinical abnormalities

TN (True Negative): The test result is negative for nonexistent clinical abnormalities.

FP (False Positive): The test result is positive for nonexistent clinical abnormalities.

FN (False Negative): The test result is negative for existent clinical abnormalities.

The dataset used in the testing state was provided to the proposed method to locate and classify the hemorrhage and calcification in the brain images. Evaluation metrics (specificity, accuracy, sensitivity, and overlap) were used to evaluate the obtained results. The following formulas were used to determine the values of these metrics in the brain images.

$$\text{Sensitivity} = \text{TP}/(\text{TP} + \text{FN})$$

$$\text{Specificity} = \text{TN}/(\text{TN} + \text{FP})$$

$$\text{Accuracy} = (\text{TN} + \text{TP})/(\text{TN} + \text{TP} + \text{FN} + \text{FP})$$

As suggested by the above equations, sensitivity can be regarded as the amount of TPs correctly identified with the diagnostic test. It represents the adequacy of the test in detecting diseases. Specificity can be regarded as the amount of TNs correctly identified with the indicative test. It represents the adequacy of the test in identifying normal negative conditions. Accuracy is the amount of both TNs and TPs within a population. The exactness of a particular diagnostic test can be measured with accuracy. Specificity and sensitivity can be used to determine abnormal and normal cases, respectively. Correct accuracy and

classification of the proportion of correct classification to the total number of classification tests. The ANFIS classifier was tested by using some tested data and then evaluated using real data. We generated ANFIS architecture for hemorrhage and calcification detection. The ANFIS network was trained using the four extracted parameters. Fig. 6 shows the ANFIS architecture decision surface for calcification and hemorrhage detection and recognition of the four parameters, namely, contrast, energy, correlation, and homogeneity.

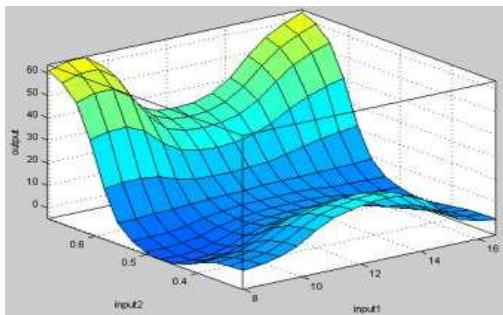


Fig. 6. (a) ANFIS decision surface for hemorrhage and calcification classification

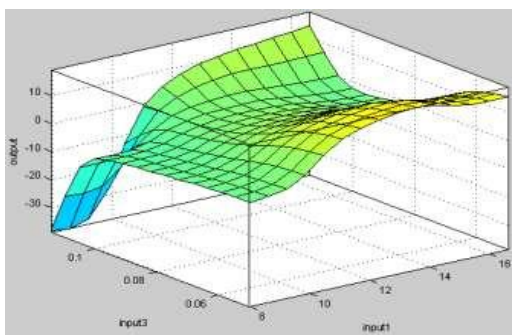


Fig. 6. (b) ANFIS decision surface for hemorrhage and calcification classification

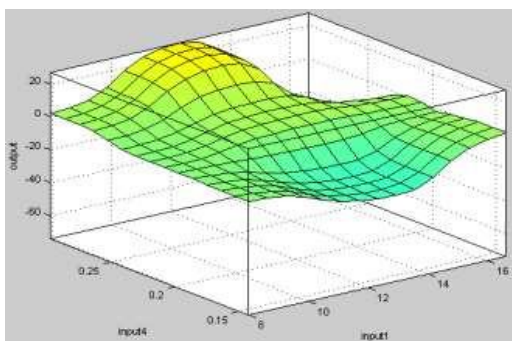


Fig. 6. (c) ANFIS decision surface for hemorrhage and calcification classification

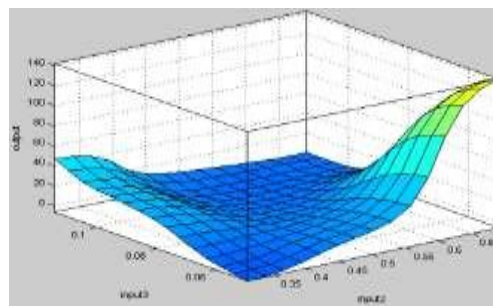


Fig. 6. (d) ANFIS decision surface for hemorrhage and calcification classification

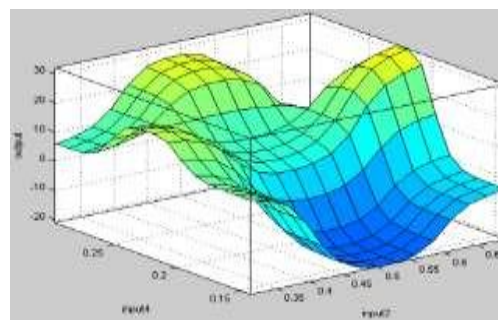


Fig. 6. (e) ANFIS decision surface for hemorrhage and calcification classification

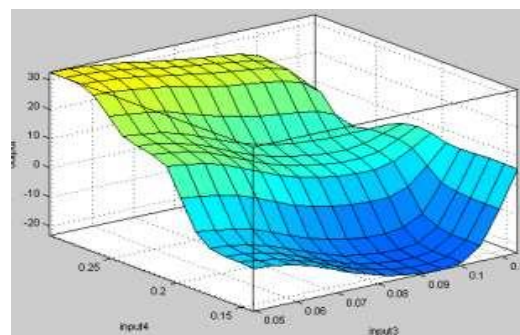


Fig. 6. (f) ANFIS decision surface for hemorrhage and calcification classification

ANFIS is useful in addressing the aforementioned issues despite the nonlinear characteristics of the diagnostic process. ANFIS method used to classify hemorrhage diagnosis by using the results for 60 records. The performance of the proposed approach under different resolutions is better than that of the other methods. It also performs better than the other algorithms when used in segmentation for dissimilar types of medical images, such as lungs, heart, and chest with single and multiple bleeding patterns.

Table 5: Performance classification of training and testing datasets by ANFIS.

Evaluation metrics	Proposed Method Training Dataset	Proposed Method Testing Dataset
TN	99	99
FP	98	99
TP	1	1
FN	2	1
Specificity	99.90	98.99
Sensitivity	99.99	99.99
Accuracy	98.90	98.60
Overlap	99.00	99.39

Table 6: ANFIS and other state-of-the art methods used in performance classification based on evaluation metrics.

Classifier	Specificity (%)	Sensitivity (%)	Accuracy (%)	Overlap (%)
ANN[29]	90.23	91.31	93.41	90.78
KNN[12]	90.34	89.23	92.34	91.76
PNN[28]	92.43	92.76	90.63	89.43
ANN+LVQ[31]	91.56	90.56	91.55	88.67
BPN[32]	88.23	93.45	92.33	92.13
DWT+PCA+ANN[13]	86.47	91.54	87.16	91.40
Proposed	98.99	99.99	98.60	99.39

To evaluate our proposed classifier, we compared our method with state-of-the-art classifiers, namely, ANN, KNN, PNN, ANN+LVQ, BPN, and DWT+PCA+ANN. For a supplementary analysis of the obtained results, the hemorrhagic and calcified regions of interest were manually marked by domain experts and served as ground reality. Table explains the specificity, sensitivity, accuracy, and overlapping of the hemorrhagic regions; the calcified regions were classified by means of ANN,

KNN, PNN, ANN+LVQ, BPN, and DWT+PCA+ANN. The projected segmentation process was used to verify a dataset of 60 brain images and their dissimilarity with respect to the ground reality of the hemorrhagic and calcified regions of interest.

A quantitative assessment of the evaluation metrics was performed as a supplementary analysis of the results obtained with the proposed method. Table 5 shows that our method can generate desirable classification results with respect to ground truth regions. A dataset comprising 60 brain images was used to calculate these regions. Our method demonstrated the highest accuracy, sensitivity, and specificity. The result of the performance analysis shows the high accuracy of our method in hemorrhage and calcification segmentation. Tables 4, 5, and 6 show the assessment results for the dataset consisting of 60 brain images. Table 6 shows the sensitivity range (99.99–99.99) with an average value of 99.99, specificity range (99.90–98.99) with an average value 99.44, accuracy range (98.90–98.60) with an average value of 98.75, and overlapping range (99.00–99.39) with an average value 99.19. The results in Tables 5 and 6 demonstrate that the proposed classification method significantly enhances hemorrhage and calcification detection in terms of evaluation metrics. The accuracy of our classification method is higher than that of the other state-of-the-art techniques.

5. CONCLUSION

A number of studies have been performed to detect hemorrhage. Some studies aimed to detect one or more of the three abnormal structures in brain images, namely, calcification, hemorrhage, or both. Some methods depend on the classification of brain lesions as either benign or malignant. The subjective analysis of brain images is influenced by issues caused by human errors, although it may also be affected by fatigue and other human-related factors. The present study investigated the systematic approach in hemorrhage and calcification segmentation by using the ANFIS strategy. A desirable outcome and useful information are most likely to be produced with fuzzy clustering segmentation methods. Irregular

tissues in hemorrhage and calcification can be effectively identified with the aid of AFCM techniques. The recently recommended AFCM segmentation techniques are generally applied to medical image segmentation. By applying this unsupervised segmentation algorithm, radiotherapists can reduce the effects of noise resulting from low-resolution sensors or/and from the movement of assemblies during data collection. The most important parameters can be estimated by designing an ANFIS coordination scheme, which is an important criterion in overall diagnostics. Simulations were run in MATLAB, and the results obtained were observed on the corresponding output blocks.

REFERENCES

- [1] Wu, Z., Mittal, S., Kish, K., Yu, Y., Hu, J., & Haacke, E. M. Identification of calcification with MRI using susceptibility-weighted imaging: a case study. *Journal of Magnetic Resonance Imaging*, 29(1), 177-182, 2009.
- [2] Haussen, D. C., Gaynor, B. G., Johnson, J. N., Peterson, E. C., Elhamady, M. S., Aziz-Sultan, M. A., & Yavagal, D. R. Carotid siphon calcification impact on revascularization and outcome in stroke intervention. *Clinical neurology and neurosurgery*, 120, 73-77, 2014.
- [3] Tawil, M., Wilson, J., & Wright, N. Intracranial lithography? *The British journal of radiology*, 75(894), 563-564, 2002.
- [4] de Oliveira, D. F., de Lemos, R. R., & de Oliveira, J. R. Mutations at the SLC20A2 gene and brain resilience in families with idiopathic basal ganglia calcification ("Fahr's disease"). *Frontiers in human neuroscience*, 2013.
- [5] Creasy, J. L. *Dating Neurological Injury:: A Forensic Guide for Radiologists, Other Expert Medical Witnesses, and Attorneys*: Springer, 2010.
- [6] Grannan, B. L., Yanamadala, V., Walcott, B. P., Stapleton, C. J., & Ogilvy, C. S. Repeated neurovascular imaging in subarachnoid hemorrhage when initial studies are negative. *Journal of Clinical Neuroscience*, 21(6), 993-996, 2014.
- [7] Weishaupt, D., Froehlich, J., Nanz, D., Köchli, V. D., Pruessmann, K., & Marincek, B. *How does MRI work?: an introduction to the physics and function of magnetic resonance imaging*: Springer, 2008.
- [8] Masulli, F., & Schenone, A. A fuzzy clustering based segmentation system as support to diagnosis in medical imaging. *Artificial Intelligence in Medicine*, 16(2), 129-147, 1999.
- [9] Wu, K.-L., & Yang, M.-S. Alternative c-means clustering algorithms. *Pattern recognition*, 35(10), 2267-2278, 2002.
- [10] Bharathi, K. K., Muruganand, S., & Periasamy, A.. *Digital Image Processing Based Noise Reduction Analysis of Digital Dental Xray Image Using MATLAB*. *Journal of NanoScience and NanoTechnology*, 2(1), 198-203, 2014.
- [11] Vishnuvarthanan, G., Rajasekaran, M. P., Subbaraj, P., & Vishnuvarthanan, A.. An unsupervised learning method with a clustering approach for tumor identification and tissue segmentation in magnetic resonance brain images. *Applied Soft Computing*, 38, 190-212, 2016.
- [12] Steed, T., Treiber, J., Patel, K., Taich, Z., White, N., Treiber, M., . . . Chen, C. Iterative Probabilistic Voxel Labeling: Automated Segmentation for Analysis of The Cancer Imaging Archive Glioblastoma Images. *American Journal of Neuroradiology*, 2014.
- [13] El-Dahshan, E., Salem, A.-B. M., & Younis, T. H. A hybrid technique for automatic MRI brain images classification. *Studia Univ. Babeş-Bolyai, Informatica*, 54(1), 55-57, 2009.
- [14] Zhang, Y., Brady, M., & Smith, S. Segmentation of brain MR images through a hidden Markov random field model and the expectation-maximization algorithm. *Medical Imaging, IEEE Transactions on*, 20(1), 45-57, 2001.
- [15] Saha, S., & Bandyopadhyay, S. (2007). MRI brain image segmentation by fuzzy symmetry based genetic clustering technique. Paper presented at the Evolutionary Computation, IEEE Congress on 2007.
- [16] Jaffar, M. A., Zia, S., Latif, G., Mirza, A. M., Mehmood, I., Ejaz, N., & Baik, S. W. Anisotropic diffusion based brain MRI segmentation and 3D reconstruction. *International Journal of Computational Intelligence Systems*, 5(3), 494-504, 2012.
- [17] Li, B., Chen, W., & Wang, D. An improved FCM algorithm incorporating spatial information for image segmentation. Paper presented at the Computer Science and Computational Technology, 2008. ISCSCT'08. International Symposium on. 2008.
- [18] Ahmed, M. M., & Mohamad, D. B., Segmentation of brain MR images for

- tumor extraction by combining kmeans clustering and perona-malik anisotropic diffusion model. *International Journal of Image Processing*,**2**(1): p. 27-34, 2008.
- [19] Bezdek, J. C., Pattern recognition with fuzzy objective function algorithms. 1981: Kluwer Academic Publishers, 1981.
- [20] Wang, P., & Wang, H. A modified FCM algorithm for MRI brain image segmentation. in *Future BioMedical Information Engineering*, 2008. FBIE'08. International Seminar on. IEEE. 2008.
- [21] Dubey, Y. K., Mushrif, M. M., & Mitra, K, Semi-automatic segmentation of MRI Brain tumor. *ICGST-GVIP Journal*,**9**(4): p. 33-40, 2009.
- [22] Yang, M.-S., A survey of fuzzy clustering. *Mathematical and Computer modelling*,**18**(11): p. 1-16, 1993.
- [23] Zadeh, L.A., Fuzzy sets. *Information and control*,**8**(3): p. 338-353, 1965.
- [24] Phillips II, W., Velthuisen, R., Phuphanich, S., Hall, L., Clarke, L., & Silbiger, M., Application of fuzzy c-means segmentation technique for tissue differentiation in MR images of a hemorrhagic glioblastoma multiforme. *Magnetic resonance imaging*,**13**(2): p. 277-290, 1995.
- [25] Lin, J.-S., Cheng, K.-S., & Mao, C.-W., Segmentation of multispectral magnetic resonance image using penalized fuzzy competitive learning network. *Computers and Biomedical Research*,**29**(4): p. 314-326, 1996.
- [26] Suckling, J., Sigmundsson, T., Greenwood, K., & Bullmore, E, A modified fuzzy clustering algorithm for operator independent brain tissue classification of dual echo MR images. *Magnetic resonance imaging*,**17**(7): p. 1065-1076, 1999.
- [27] Arif, M., Abdullah, N. A., Phalianakote, S. K., Ramli, N., & Elahi, M. Maximizing Information of Multimodality Brain Image Fusion Using Curvelet Transform with Genetic Algorithm. in *Computer Assisted System in Health (CASH)*, 2014 International Conference on. IEEE. 2014.
- [28] Nanthagopal, A. P., & Rajamony, R. S., Classification of benign and malignant brain tumor CT images using wavelet texture parameters and neural network classifier. *Journal of Visualization*,**16**(1): p. 19-28, 2013.
- [29] Varghese, T., Kumari, R. S., Mathuranath, P., & Singh, N. A. Discrimination between Alzheimer's Disease, Mild Cognitive Impairment and Normal Aging Using ANN Based MR Brain Image Segmentation. in *Proceedings of the International Conference on Frontiers of Intelligent Computing: Theory and Applications (FICTA)* Springer, 2013-2014.
- [30] Dubey, Y. K., Mushrif, M. M., & Mitra, K., Segmentation of brain MR images using rough set based intuitionistic fuzzy clustering. *Biocybernetics and Biomedical Engineering*, 2016.
- [31] Melin, P., Amezcua, J., Valdez, F., & Castillo, O., A new neural network model based on the LVQ algorithm for multi-class classification of arrhythmias. *Information Sciences*,**279**: p. 483-497, 2014.
- [32] Rajakeerthana, K., Velayutham, C., & Thangavel, K., Mammogram Image Classification Using Rough Neural Network, in *Computational Intelligence, Cyber Security and Computational Models.*, Springer. p. 133-138, 2014.